Journal of Volcanology and Geothermal Research xxx (2015) xxx–xxx

Contents lists available at ScienceDirect

Journal of Volcanology and Geothermal Research

journal homepage: www.elsevier.com/locate/jvolgeores

Dike model for the 2012–2013 Tolbachik eruption constrained by satellite radar interferometry observations

Paul Lundgren [a,*], Alexey Kiryukhin [b], Pietro Milillo [a,c], Sergey Samsonov [d]

[a] Jet Propulsion Laboratory, California Institute of Technology, 4800 Oak Grove Drive, Pasadena, CA 91109, USA
[b] Institute of Volcanology & Seismology FEB RAS, Piip 9, Petropavlovsk-Kamchatsky 683006, Russia
[c] Università degli Studi della Basilicata, Potenza, Italy
[d] Canada Centre for Mapping and Earth Observation, Natural Resources Canada, 560 Rochester Street, Ottawa, ON K1A 0E4, Canada

ARTICLE INFO

Article history:
Received 22 December 2014
Accepted 16 May 2015
Available online xxxx

Keywords:
InSAR
Dike modeling
Tolbachik volcano

ABSTRACT

A large dike intrusion and fissure eruption lasting 9 months began on November 27, 2013, beneath the south flank of Tolbachik Volcano, Kamchatka, Russia. The eruption was the most recent at Tolbachik since the Great Tolbachik Eruption from 1975 to 1976. The 2012 eruption was preceded by more than 6 months of seismicity that clustered beneath the east flank of the volcano along a NW–SE trend. Seismicity increased dramatically before the eruption, with propagation of the seismicity from the central volcano conduit in the final hours. We use interferometric synthetic aperture radar (InSAR) to compute relative displacement images (interferograms) for SAR data pairs spanning the eruption. We use satellite SAR data from the Canadian Space Agency's RADARSAT-2 and from the Italian Space Agency's COSMO-SkyMed missions. Data are modeled first through a Markov Chain Monte Carlo solution for a single tensile dislocation (dike). We then use a boundary element method that includes topography to model a distributed dike-opening model. We find the best-fitting dike dips 80° to the WNW with maximum opening of 6–8 m, localized in the near surface and more broadly distributed in distinct regions up to 3 km beneath the surface, which varies from 1 to 2 km elevation for the eruptive fissures. The distribution of dike opening and its correspondence with co-diking seismicity suggests that the dike propagated radially from Tolbachik's central conduit.

1. Introduction

The flank eruption of Tolbachik Volcano began on 27 November 2012 and was its first eruption since the Great Tolbachik Eruption (GTE) of 1975–1976 [Edwards et al., 2013]. The eruption lasted through August 2013 and was located higher up-slope Tolbachik than the previous eruption (Fig. 1). Plosky Tolbachik is the largest active volcano in the southwest sector of the Kluchevskaya volcano group, featuring a large summit caldera that was formed during the early Holocene and coincided with the appearance of subalkaline aluminous basalts that are similar to those found in dike intrusions to the SW [Dvigalo et al., 1991]. These SW dikes coincide with fissure eruptions, such as those in 1975–1976 and 2012–2013, and consist of monogenetic cinder cones and large basaltic lava flow fields that comprise the New Tolbachik Volcanoes or Tolbachik Dol (Valley). During the 1975–1976 GTE lava flowed from two areas located 18 and 36 km SSW of Plosky Tolbachik summit [Fedotov et al., 1991].

In order to understand the dynamics of dike propagation, volume change [Segall et al., 2001; Rivalta and Segall, 2008; Rivalta, 2010] and the processes within the feeding system of large fissure eruptions it is important to constrain the total opening of the dike, its geometry, shape, and differential opening along strike and at depth. Geodetic data can be used to constrain dike geometry [Owen et al., 2000; Wright et al., 2006], kinematics [Bagnardi et al., 2013] and when combined with seismicity production, models can constrain dike propagation dynamics [Segall et al., 2013]. The advent of interferometric synthetic aperture radar (InSAR) has enabled more detailed modeling of dike opening, and when sampled during and after fissure eruptions can provide a more detailed kinematic representation of dike growth and origin [Bagnardi et al., 2013; Lundgren et al., 2013].

We use satellite InSAR to compute maps of relative surface deformation. InSAR line-of-sight (LOS) displacement data, as well as the locations of eruptive fissures, are used to constrain numerical inverse models for the dike location, dip, and distributed opening. We develop a distributed dike-opening model in a model domain that incorporates the volcano's topography to provide a more comprehensive model for total dike opening that we then compare to the distribution of seismicity before and during the eruption.

2. Data

InSAR is now a well-established method for computing images (interferograms) of relative surface deformation projected into the

* Corresponding author. Tel.: +1 818 354 1795; fax: +1 818 354 9476.
E-mail address: paul.lundgren@jpl.nasa.gov (P. Lundgren).

http://dx.doi.org/10.1016/j.jvolgeores.2015.05.011
0377-0273/

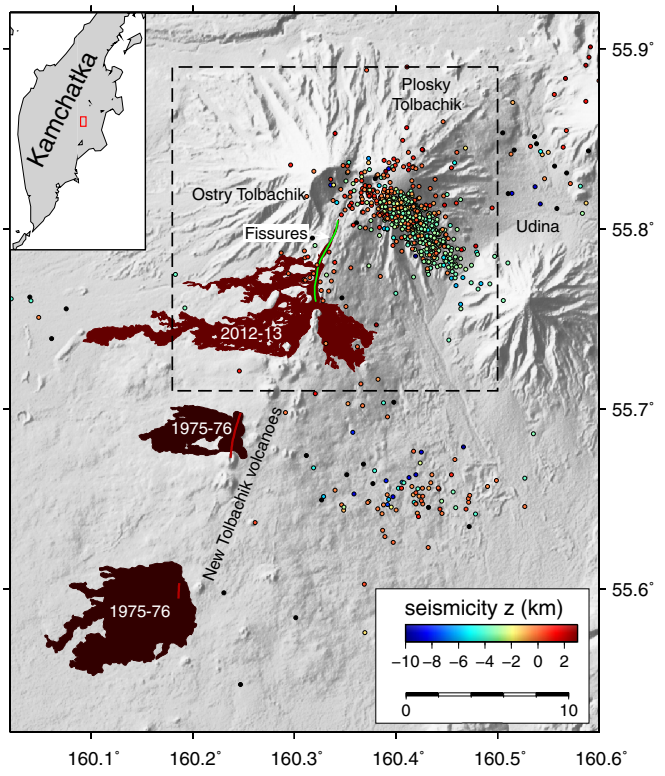

Fig. 1. Map of study area plotted using Generic Mapping Tools (Wessel and Smith, 1995). Dark red areas show the extent of the 2012–2013 lava flows [Volynets et al., 2013]. Black areas indicate lava flows from the 1975 to 1976 Great Tolbachik Eruption. Eruptive fissures (green line) derived from the 2012 to 2013 lava flows and from Edwards et al. (2013). Seismicity is for the second half of 2012 (from the Kamchatka Branch Geophysical Survey, Russian Academy of Science). Dashed line box indicates the 20 × 20 km area shown for the dike source model plots. Upper left inset shows the detailed map area (red box) with respect to the Kamchatka Peninsula, Russia. (For interpretation of the references to color in this figure legend, the reader is referred to the web version of this article.)

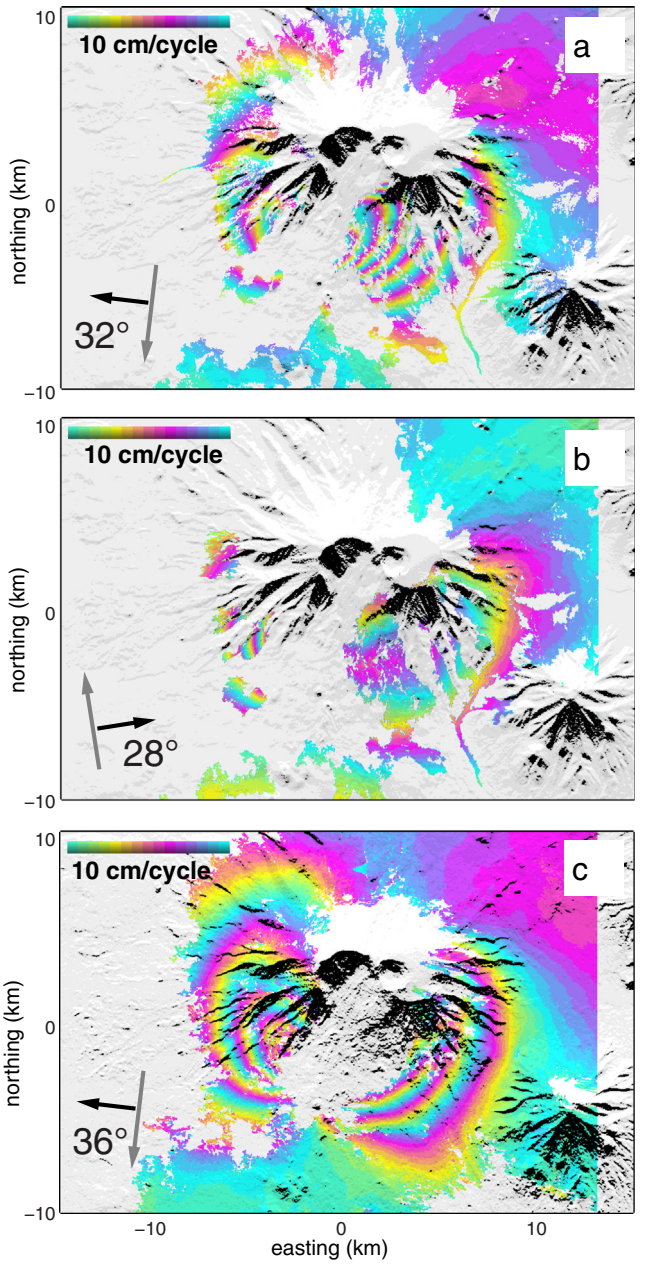

Fig. 2. InSAR data used in this study. Each color cycle shows 10 cm line-of-sight (LOS) deformation, where the satellite LOS 'look' direction is indicated by the black arrow, the approximate ground incidence angle (in degrees) and the satellite heading direction by the gray arrow. (a) COSMO-SkyMed descending track interferogram from 2012/09/09 to 2013/08/30. (b) COSMO-SkyMed ascending track interferogram from 2012/08/06 to 2013/08/13. (c) RADARSAT-2 descending track interferogram from 2012/06/12 to 2014/06/02. (For interpretation of the references to color in this figure legend, the reader is referred to the web version of this article.)

radar LOS. Satellite SAR systems typically collect strip-map data over 40–100 km wide swaths, which are well suited to cover entire volcanoes, with a typical pixel sampling from 2 to 100 m at sub-centimeter precision [Rosen et al., 2000].

We use SAR data from the Canadian Space Agency's RADARSAT-2 (RSAT2) C-band (5.6 cm wavelength) satellite, and the Italian Space Agency's COSMO-SkyMed (CSK) constellation of four X-band (3.1 cm wavelength) satellites. Due to the long winter and high topography of Tolbachik Volcano, interferograms can only be formed with high coherence during the late summer (August through the first half of September, generally). Therefore, in order to measure the deformation associated with the eruption it was necessary to compute interferograms from summer 2012 to summer 2013 [Fig. 2]. This precludes capturing any dike transient behavior through sustained SAR acquisitions during the eruption [e.g. Lundgren et al., 2013], but it does allow us to span the entire eruption and constrain its total dike opening.

The SAR data were processed using two different software packages. The RADARSAT-2 data were processed at the Canada Centre for Remote Sensing using the Gamma processing package [Wegmuller and Werner, 1997].

The CSK data were processed at the Jet Propulsion Laboratory (JPL) using the JPL developed InSAR Scientific Computing Environment (ISCE) open source software package. We used the Shuttle Radar Topography Mission (SRTM) 30 m digital elevation model (DEM) to remove the topographic effect and form the differential interferograms. CSK interferograms were filtered using a power spectrum filter [Goldstein and Werner, 1998] with an exponent of 0.5. The large deformation combined with the topography of the volcano, which features steep ravines radiating from the summit, makes automated phase unwrapping difficult. We used the branch-cut unwrapper [Goldstein et al., 1988], implementing numerous "bridges" to manually connect isolated areas of coherent phase in order to expand the unwrapping.

We use the three best interferograms for the RSAT2 descending, and the CSK descending and ascending tracks (Fig. 2). In the case of the RSAT2 interferogram coherence was improved by using post-eruption SAR data from June 2014, which had a smaller perpendicular orbital baseline that improved coherence in areas of higher topography.

For modeling purposes interferograms are cropped and down-sampled to provide a computationally practical number of data points for use in the numerical modeling. We down-sample the interferograms using a model-based quad-tree approach [Lohman and Simons, 2005].

Please cite this article as: Lundgren, P., et al., Dike model for the 2012–2013 Tolbachik eruption constrained by satellite radar interferometry observations, J. Volcanol. Geotherm. Res. (2015), http://dx.doi.org/10.1016/j.jvolgeores.2015.05.011

We use a vertical dike model to down-sample the data to 650, 604, and 849 samples for the RSAT2, CSK ascending, and CSK descending, respectively. Each quad-tree point is computed from the mean value of the original coherent unwrapped phase within each square area of pixels. Standard deviations for each point are also computed and are generally in the range from 1 to 5 mm.

3. Modeling

We use two approaches to model the dike. First we blindly estimate the parameters for a single tensile dislocation. This serves two purposes: 1) it gives a baseline solution to evaluate the ability of a simple source to fit the data; and 2) it provides a basis for testing more realistic, complex dike opening models and for comparing their results and improvement in fitting the data.

3.1. Simple model

The best fitting geometry and opening amount for a rectangular dislocation [Okada, 1985] is solved for using a Markov chain Monte Carlo (MCMC) approach [Fukuda and Johnson, 2010], developed at JPL and written in MATLAB©. Probability density functions are determined from histograms of retained solutions for each parameter (Fig. S1). In order to adequately sample the parameter probability distributions [Mosegaard and Tarantola, 2002] a large number of samples are required, typically on order one million [Malinverno, 2002].

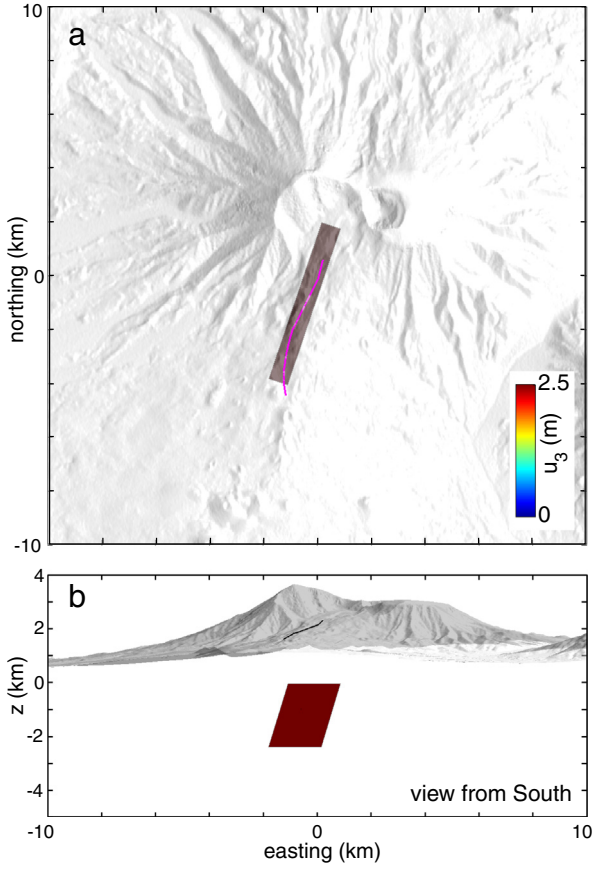

Fig. 3. Markov chain Monte Carlo solution for a single tensile dislocation (dark red rectangle — the color corresponds to the maximum color of the scale bar, $u_3 = 2.5$ m) as seen in this map view (a) and as a side view from the South. The dike parameter probability density functions are given in Fig. S1 and the model fit to the data are shown in Fig. S2. The dike's top edge is ESE of the mapped fissures (magenta line) and it dips 72° to the WNW with width 2.5 km, and length 6.1 km. Uniform opening displacement (u_3) is 2.5 m. (For interpretation of the references to color in this figure legend, the reader is referred to the web version of this article.)

Using a reasonable starting model based on the mapped fissure locations, we ran the MCMC solution until we obtained one million retained solutions, since not all solutions are retained if they do not improve the solution fit to the data, though some trial models that increase data misfit are randomly retained. The first one hundred thousand solutions were thrown out during the 'burn-in' phase and parameter distributions determined for the remaining solutions. The peak in the distribution is chosen as the most probable parameter value with 95% confidence intervals computed (Fig. S1). The resulting model is shown in map view (Fig. 3) and the fit of the synthetic data to the observed is shown in Fig. S2.

From these results we see that a single tensile dislocation with 2.5 m opening extending from the surface to 2.5 km depth at a dip angle of 72° provides a good fit to the data. The strike of the dike compares well with the observed eruption fissures, although the location is offset to the east, especially with respect to the northern, higher fissure zone. The inaccurate position of the dike may result from a lack of coherent InSAR data adjacent the eruptive fissures and from using Greens functions for an elastic half-space to model the dike, rather than including topographic effects and using a more accurate rheology, which can give rise to miss-modeled source locations [Masterlark et al., 2010].

3.2. Topography model

In order to better resolve the amount and distribution of dike opening we take the simple model derived above and expand it to a multi-patch dislocation dike and solve for the distributed opening. In the case of Tolbachik volcano there is the added complexity of the topography, which can modify the pattern of surface deformation [Williams and Wadge, 2000].

To account for topography and model the dike we use the boundary element method (BEM) software POLY3D [Thomas, 1993], which can model arbitrary polygonal dislocations, imposing either displacement or traction boundary conditions on each polygon and constructing planar or curved surfaces or volumes from multi-patch connected polygons. In order to simulate topographic effects we drape a large (30 km radius) circular crack with zero traction boundary conditions over the SRTM 30 m DEM, similar to previous studies [Walter and Amelung, 2006; Salzer et al., 2014]. Surface displacements are derived from the underside crack displacements. We model the dike using the MCMC solution dike as our starting model and extend it to the surface crack without piercing it. We keep the lower edge of the dike at 2.5 km depth (beneath sea level) and then adjust the lateral (E–W) location of the dike in order to align it with the center of the fissure trace.

The MCMC derived dislocation is extended in length to 10 km, from a depth of 2.4 km below sea level to the topography surface (around +2 km), and divided into 240 patches (20 × 12 columns and rows, respectively). After solving for unit opening Greens functions for each patch, a non-negative least-squares inversion is used to solve for the dike-opening model. In order to suppress overly rough dike opening with respect to the effective resolution we add a Laplacian smoothing submatrix to the inverse problem design matrix [Jónsson et al., 2002].

Once we have gone from a half-space solution to the topography corrected solution with an irregular distributed slip there are two parameters to determine before we decide on the most reasonable model. First, there is the potential that the initial MCMC geometry may not be correct: the best fitting geometry for a simple single dislocation model might find an incorrect geometry from that for a distributed dike in a half-space. Second, on top of introducing opening irregularity, we have also taken into account topography (though always in an elastic medium). We have taken three approaches to empirically derive reasonable values for both the dip and the amount of dike opening smoothing. To consider the effects that the Laplacian smoothing parameter Gamma [Jónsson et al., 2002; Fukuda and Johnson, 2010], has on the slip distribution and the fit of the modeled displacements to the observed ones we consider two approaches. First we perform a

Please cite this article as: Lundgren, P., et al., Dike model for the 2012–2013 Tolbachik eruption constrained by satellite radar interferometry observations, J. Volcanol. Geotherm. Res. (2015), http://dx.doi.org/10.1016/j.jvolgeores.2015.05.011

"checkerboard" test, generating synthetic data plus added noise for an alternating pattern of unit opening on the dike and then solve for the model opening using a range of smoothing parameters (Fig. 4). From these solutions we see that the smoothing parameter, Gamma, produces a highly smoothed solution deeper than about 1 km beneath the surface. As Gamma is increased smoothing is reduced and deeper squares emerge somewhat, though in an uneven manner and often with significant smearing with depth. Even at Gamma equal to 150 there is improving detail while maintaining maximum opening values only slightly above the actual 1-meter true model values.

The second approach to determining the optimal smoothing value is to compute the "L"-curve [Jónsson et al., 2002] of reduction of misfit versus opening roughness (Fig. 5a). However, the "corner" in the curve is subjective with the apparent maximum curvature somewhat dependent on the range of Gamma values chosen. Here we see that a value around 20 would appear optimal, whereas the checkerboard test would suggest a higher value of Gamma (rougher solution) is warranted.

The simple dike model found a strike that is in agreement with the observed eruption fissures [Edwards et al., 2013]. Therefore the only question regards the dip of the dike (since the length and width can be reasonably extended for a distributed model and the location is aligned to the mapped fissures). To check the single, half-space dislocation dip for the distributed opening topography model we computed a series of models with dip angle varying from 70 to 90+° (Fig. 5b), dips beyond 90° give even larger residual sum of squares (RSS) values that are not shown here. We found that the best fitting dip was at 80°, closer to vertical than the MCMC half-space solution (not shown). It is worth noting that in our initial topography corrected model we had placed the dike approximately 200 m to the west, and in that scenario the best fitting dike dip was vertical. This can be explained because as the dike shifts to the east its increasing proximity (and therefore deformation magnitude) to InSAR displacements immediately to the east increases with respect to those data points to the west of the dike. To compensate the dike dip rotates toward the west, thus increasing displacements to the west and decreasing those to the east.

4. Results

Distributed dike models were computed for a wide range of smoothing parameter at a dip of 80° with the results for Gamma values of 20, 50, and 150 (Fig. 6). These results show a graceful degradation in the amplitude of the opening at depth while maintaining the essential distribution of opening. The models appear to conserve total dike volume for reasonable ranges of smoothing, which is 44 million cubic meters (MCM) for each solution (Fig. 6). Locations of maximum surface opening remain roughly constant (not surprising given the checkerboard model) with two maxima 1.5–3 km beneath the surface separated along strike by a similar amount. As Gamma increases (less smoothing) the amount of opening in these two areas increases, and decreases in area as would be expected. Each of the two areas of concentrated opening at depth appear to connect to the surface and to each other.

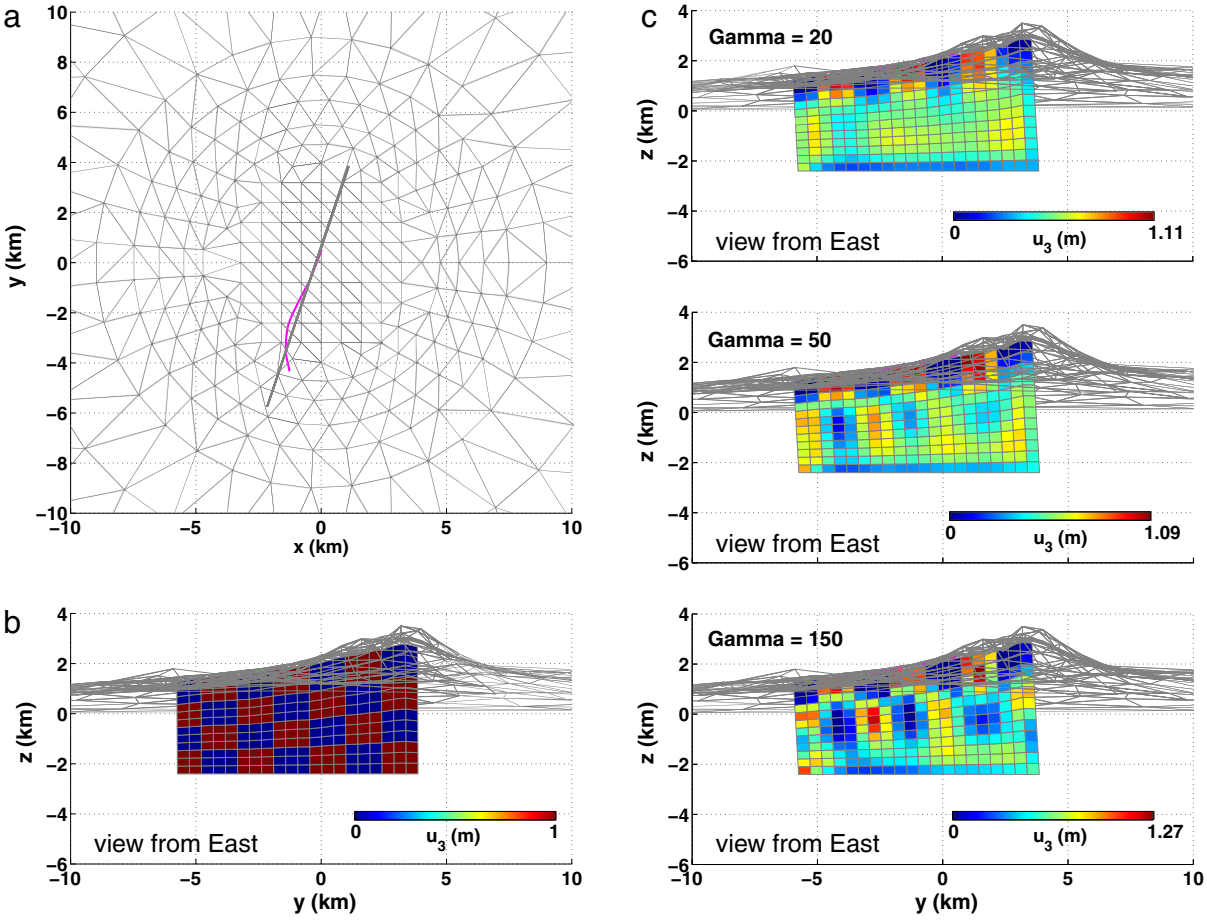

Fig. 4. Boundary element topography mesh. checkerboard resolution test inputs, and results for three different smoothing factors (Gamma). (a) Map view of central 10 × 10 km portion of the mesh with the magenta line indicating the center of the fissure. The dike dips 89° (near vertical). (b) View from the east of the checkerboard pattern of opening. (c) Retrieved opening values after adding random noise based on the normally distributed data uncertainties to the synthetic data and inverting for different smoothing factors (Gamma), ranging from greater (Gamma = 20) to lesser smoothing (Gamma = 150).

Please cite this article as: Lundgren, P., et al., Dike model for the 2012–2013 Tolbachik eruption constrained by satellite radar interferometry observations, J. Volcanol. Geotherm. Res. (2015), http://dx.doi.org/10.1016/j.jvolgeores.2015.05.011

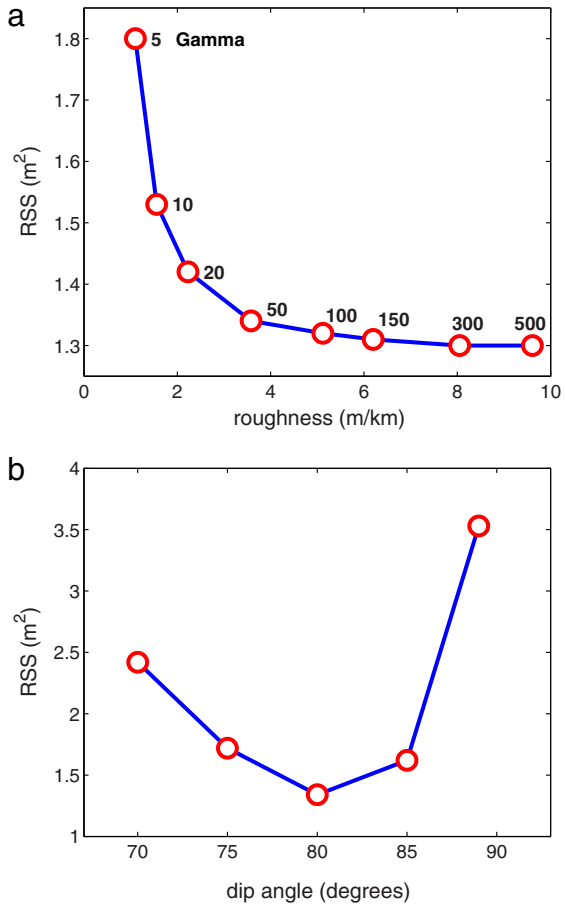

Fig. 5. (a) Residual sum of squares (RSS) model misfit versus opening model solution roughness (u_3 gradient) as a function of Gamma. Less smoothing (larger Gamma) improves the fit to the data but with diminishing returns beyond the "corner" at Gamma equal to 20 to 50. (b) RSS versus dike dip angle (90° = vertical) for the boundary element topography model. This shows that an 80° dike provides the best data fit.

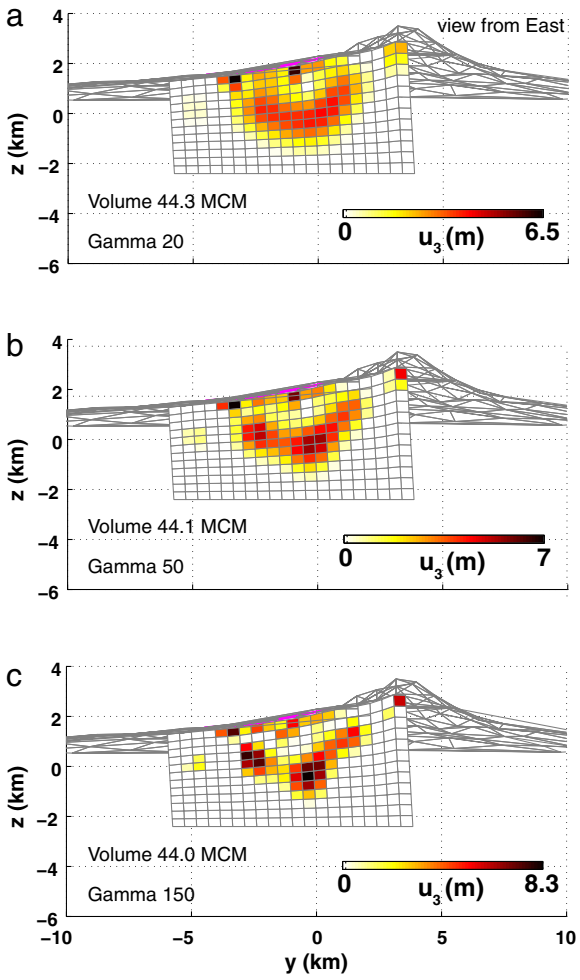

Fig. 6. Opening solutions for an 80° dike at three different smoothing values (Gamma). The dike volume is also given for each model in units of million cubic meters (MCM) or 10^6 m^3.

The comparison of observed, synthetic, and residual data for the Gamma = 50 model (Fig. 7) shows low residuals, with some (Fig. 7c) likely due to unwrapping errors. Though not grossly improved with respect to the MCMC solution residuals (Fig. S2) some areas of systematic misfit in the near-fissure data are clearly reduced in the distributed opening model.

5. Discussion

The 2012–2013 Tolbachik flank eruption is the first eruption since the Great Tolbachik fissure eruption that lasted for 18 months from 1975 to 1976 and resulted in a large volume of lava effusion from the lower south flank (Fig. 1). Here we discuss our dike model results with respect to other observations for the 2012–2013 eruption, such as seismicity and the locations of lava effusion, as well as comparisons with the Great Tolbachik fissure eruption.

5.1. Distributed dike opening model

Our dike model suggests an irregular dike consisting of two areas of greater opening at roughly +1 to −2 km relative to sea level, separated from the areas of shallow surface opening. Dike opening varies from roughly 2 to 4 m to as high as 6 to 8 m in the areas of highest opening. It should be noted that the very concentrated opening near the surface remains relatively stable with reduced smoothing (Fig. 6), whereas as smoothing is reduced the deeper opening increases and localizes. Field observations of exposed dikes over the north flank of Tolbachik range from 1 to 10 m, with most below 5 m thickness (Churikova et al., 2014). This is roughly in agreement with our modeled results.

We take the portions of the dike that opened in the finite dike models for Gamma equal to 50 or 150 (Fig. 6) and use POLY3D to solve for a constant pressure change in the dike (Fig. 8). For each model the solution for a constant unit tensile traction is solved for the irregular crack, with the best-fitting pressure scale factor calculated through a simple linear least-squares inversion. The modeled data show greater misfit in the near-field CSK data (Fig. S3) that likely reflects differences between the dislocation-based solution (Fig. 6) that allows much greater opening heterogeneity than the irregular tensile crack solutions (Fig. 8). However, there are likely more optimal crack shapes that would better fit the data if we used a direct estimation of the crack shape that best fit the data [Lundgren and Lu, 2006; Yun et al., 2006]. For a given crack shape (Fig. 8) the resulting opening of the dike depends on the breadth of the dike area, whereas the excess pressure change (ΔP) is proportional to the shear modulus (μ) of the elastic medium [Thomas, 1993]. As the dike becomes more irregular the resultant opening and ΔP required to fit the data increase. In order not to exceed the expected excess pressure required to cause fracture (<10 MPa) for basaltic systems [Gudmundsson, 2012] suggests that more compliant (lower μ) materials are required at shallower depths to allow for greater amounts of dike opening.

Please cite this article as: Lundgren, P., et al., Dike model for the 2012–2013 Tolbachik eruption constrained by satellite radar interferometry observations, J. Volcanol. Geotherm. Res. (2015), http://dx.doi.org/10.1016/j.jvolgeores.2015.05.011

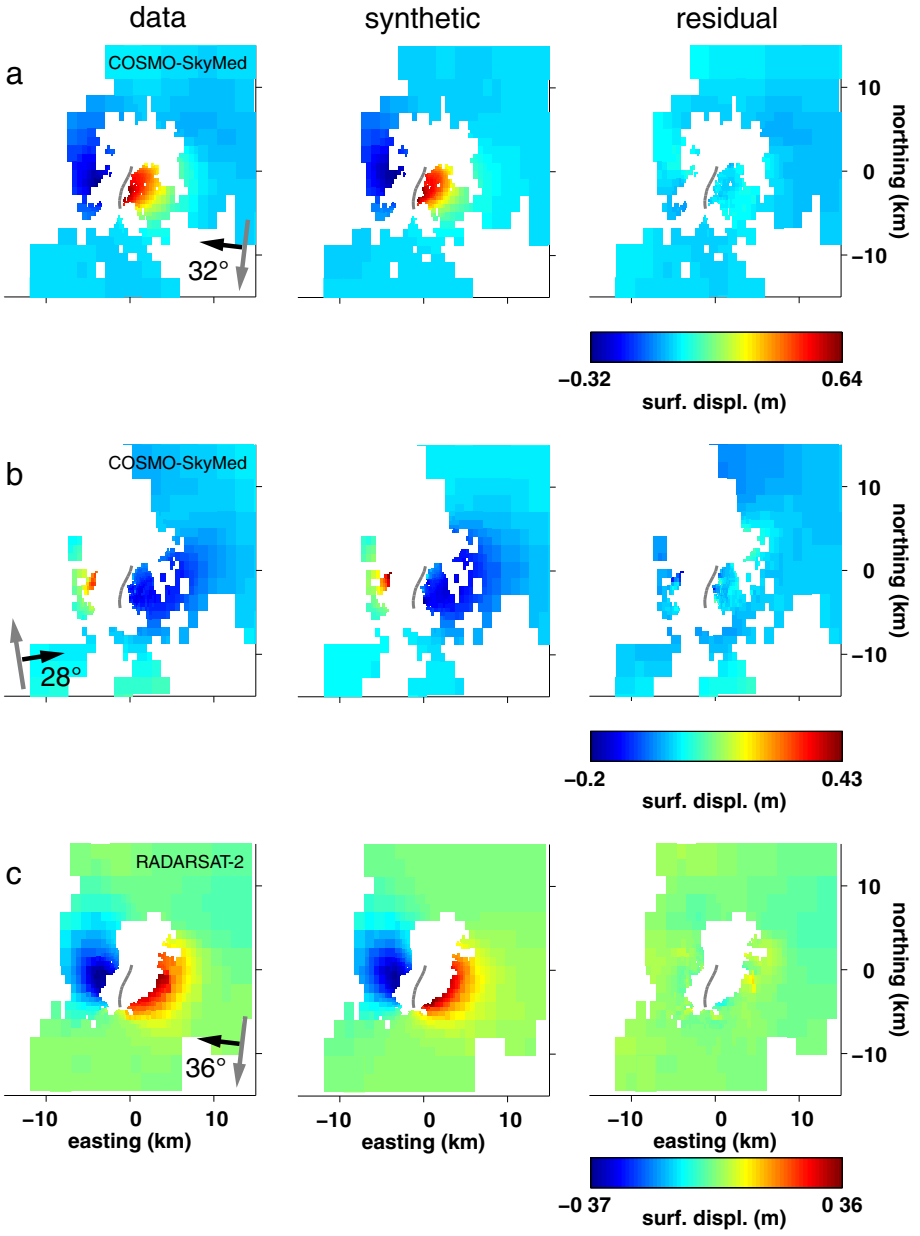

Fig. 7. Observed, synthetic, and residual down-sampled InSAR data from the three interferograms shown in Fig. 2 for the model with Gamma 50.

5.2. Comparison with seismicity

We compare the seismicity preceding and during the 2012 eruption (Fig. 1) with the distributed dike model (Fig. 9). The seismicity for the period July 1, 2012 until January 1, 2013 (Fig. 1) shows a large area of shallow seismicity mostly to the ESE of Plosky Tolbachik in the direction of Udina Volcano. In the roughly 5 months prior to the dike intrusion we see that the seismicity ESE of Tolbachik starts slowly in July 2012 and builds steadily into late November 2012 (Fig. 9a). The seismicity (from the Kamchatka Branch Geophysical Survey, Russian Academy of Science) does not show any particular spatial or temporal distribution during this time, nor is there any significant seismicity in the location of the future dike intrusion. Taken at face value, the elongated seismicity cluster is centered at two distinct depth horizons, one at 3 km and the other around sea level (Fig. 9a).

In Fig. 9b we show the hourly seismicity numbers and locations for November 25–27, 2012, with the dike intrusion occurring between 7 and 8 AM (UTC) on November 27. After 8:00 AM the seismicity drops precipitously and throughout the lava effusion phase remains low. During the final 2 days before the eruption there is a strong increase in seismicity in the elongated cluster of seismicity ESE of Tolbachik summit. Although noisy, the seismicity in the day prior to the dike intrusion does tend to be predominantly in the deeper depth horizon ESE of Tolbachik, occurring at shallower depth as time progresses toward the time of the dike intrusion. On November 27, in the final half hour from 7:25 to 7:57 UTC during the dike intrusion (Fig. 9b) seismicity is clustered adjacent to the southern portion of the large shallow dike opening. It is worth noting that although the seismicity associated with the dike is not tightly aligned with the dike in map view, it does correspond crudely with the areas of maximum opening at roughly 1–2 km beneath the topographic surface. But given the relatively few events located near the dike it is unclear their relation to the dike and whether they should lie beneath the lower limit of the dike as expected from laterally propagating dike models [Segall et al., 2013]. An alternative model considers the seismicity beneath the ESE flank of Plosky Tolbachik a result of ESE oriented dikes before the eruption that changed the local stresses and created the conditions for both

Please cite this article as: Lundgren, P., et al., Dike model for the 2012–2013 Tolbachik eruption constrained by satellite radar interferometry observations, J. Volcanol. Geotherm. Res. (2015), http://dx.doi.org/10.1016/j.jvolgeores.2015.05.011

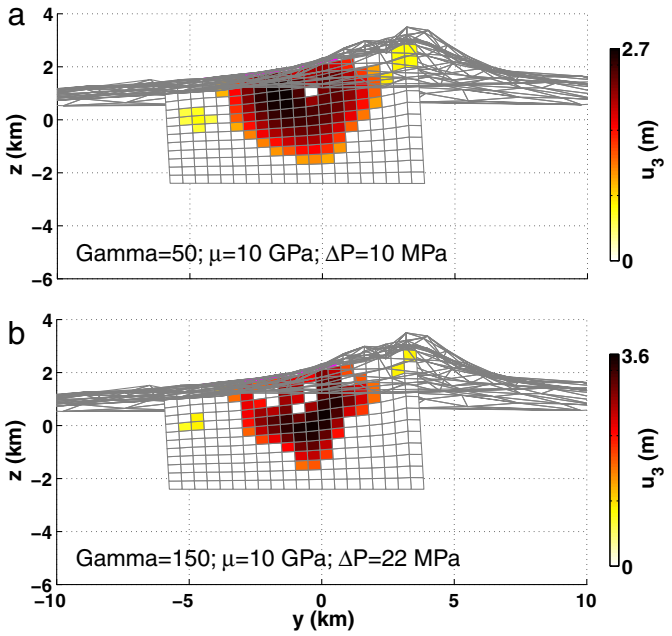

Fig. 8. Dike opening models for constant pressure change (ΔP) cracks whose shapes are based on the areas of opening found in the distributed opening models with more smoothing (a), Gamma = 50, or less smoothing (b), Gamma = 150. Fig. S3 shows the modeled surface displacements and their fit to the observed InSAR data.

horizontal sills and the SSW oriented eruptive fissures beneath the south flank of Plosky Tolbachik [Kiryukhin et al., 2015].

The main area of pre-diking seismicity ESE of Tolbachik summit suggests a shallow magma accumulation zone or reservoir, possibly aligned along a pre-existing structure that controls the alignment of the Tolbachik and Udina volcanoes. We do not find evidence for any significant deflationary deformation signal in the co-eruption InSAR data. We have also looked at CSK interferograms spanning late summer 2011 to late summer 2012 to see if there is evidence of inflation during this time period. The CSK scenes are centered on the Klyuchevskoy group to the NE and only reach the lower NE flank of Plosky Tolbachik. We do not see any apparent deformation extending into the area covered by the SAR data, but this is not conclusive depending on the magnitude of the deformation. Instead there is evidence from GPS sites located SW of Bezymianny volcano, more than 20 km NE of the Tolbachik seismicity that gives NE directed horizontal displacements followed by much larger SW directed co-eruption displacements due to dike deformation and/or deflation of the ESE Tolbachik source [Gordeev et al., 2014]. There is also a non-linear increase in seismicity with time such that most of it occurs after September 2012 (Fig. 9a). The lack of significant co-eruptive deformation seen in the InSAR data suggests that significant deformation resolvable by InSAR (i.e. centimeter level) and large enough relative to the very large dike intrusion deformation must have occurred as inflation within the 2 months prior to the eruption and deflation accompanying the eruption. Under this scenario the co-eruptive, 1-year interferograms would show no net deformation due to inflation/deflation of a magma reservoir associated with the SE Tolbachik seismicity area. Such a scenario was found for the 2011 Kilauea fissure eruption where most of the inflation occurred starting a few months before the eruption, with rapid co-eruptive deflation of the caldera over 10 km away from the dike [Lundgren et al., 2013].

We should bear in mind that accurate seismicity locations, even in well-instrumented volcanoes such as Kilauea, Hawaii, require state of the art seismic tomography and relocation methods in order to resolve highly focused, discrete linear or planar distributions of seismicity from otherwise diffuse seismicity [Shearer et al., 2005; Matoza et al., 2013; Lin et al., 2014]. Lacking background stress measurements we are not able to interpret the double-layered seismicity distribution ESE of Plosky Tolbachik volcano in terms of the relative vertical versus horizontal stress magnitudes that would promote sill rather than dike formation [Zoback, 2010]. Nevertheless, the ellipsoidal cluster of seismicity ESE of Plosky Tolbachik in the months leading up to the dike intrusion and eruption suggests one or more sill-like magma reservoirs. Sill formation may be due to the regional level of neutral buoyancy [Gudmundsson, 2012] and would also be facilitated by the reduction in overburden stress (σ_v) away from the center of the Plosky Tolbachik edifice [Zoback, 2010]. Whether these earthquakes are volcano tectonic events or related to interaction of the magma with a hydrothermal system is unclear.

5.3. Comparison with the Great Tolbachik Eruption

Compared to the Great Tolbachik Eruption (GTE), from 1975 to 1976, the 2012–2013 eruption occurred higher up the flank. Seismicity prior to the GTE was much stronger and from mantle depths (>25 km) and is reflected in less silica rich basalt in 1975 relative to 2012 [Edwards et al., 2013]. The greater depth is also supported through the analysis of low-frequency microseisms that found evidence for anomalous seismic velocities extending beneath the area of activity in 1975–1976, whereas the area beneath the 2012–2014 fissures showed no such anomalies prior to the eruption [Kugaenko et al., 2013; Kugaenko et al., 2014].

Based on petrochemical observations the GTE was also considered to have areas of greater opening, or small chambers, within the dike that allowed magma mixing during ascent [Fedotov et al., 1991]. This conceptual model for the GTE bears some resemblance to the heterogeneous opening found with the distributed opening dike model in this study. Due to the long time interval spanned by the InSAR data we are unable to examine whether the differential opening occurred simultaneously with the initial dike propagation or whether the areas of increased opening grew with time during the eruption.

Finally, we explore whether there is a relation between the location of the GTE and the 2012 dike intrusion higher up the flank. If we compute a simple model for the 1975 intrusion (meter opening over a dike corresponding to the along rift span of the two main eruption centers) (Fig. 10), we see that immediately outside the dike the coplanar rift would be in positive normal tractions. This is similar to Mauna Loa, where the relationship between past and future intrusions was examined for system memory that suggested that past dikes and earthquakes played a role in controlling future magma intrusion locations [Amelung et al., 2007]. For a simple rectangular dike (Fig. 10a) the pattern of unclamping is very simple, highest just outside the intrusion and diminishing rapidly with distance in the plane of the dike.

In addition to past intrusions in the rift zone, other sources of stress-change, including earthquakes and magma volume pressurization will also affect the amount and distribution of clamping and unclamping along the rift system [Amelung et al., 2007]. Furthermore, detailed considerations of background tectonic stresses combined with variations in gravitational potential energy can also be expected to guide dike propagation [Sigmundsson et al., 2015]. One problem, as we noted in Section 5.2, is the lack of an InSAR constrained magmatic cause for the seismic swarm beneath the SE flank of Tolbachik. Seismicity within volcanoes can occur without observed deformation, such as the Upper East Rift Zone (UERZ) of Kilauea where magma is transported from the summit caldera to the East Rift Zone effusion or during diking events. Perhaps more similar to Tolbachik is the ongoing seismic swarm just south of dormant Chiles volcano on the Colombia–Ecuador border [Lundgren et al., 2015a] in which more than 100,000 events occurred during October 2014 alone but with very small deformation (cm-level) and as yet no eruption. In the case of Kilauea's UERZ this represents a very open transport system. The Chiles system is the complete opposite, presumably, given that the most recent activity there is older than at least 10,000 and perhaps greater than 100,000 years ago [P. Mothes,

Please cite this article as: Lundgren, P., et al., Dike model for the 2012–2013 Tolbachik eruption constrained by satellite radar interferometry observations, J. Volcanol. Geotherm. Res. (2015), http://dx.doi.org/10.1016/j.jvolgeores.2015.05.011

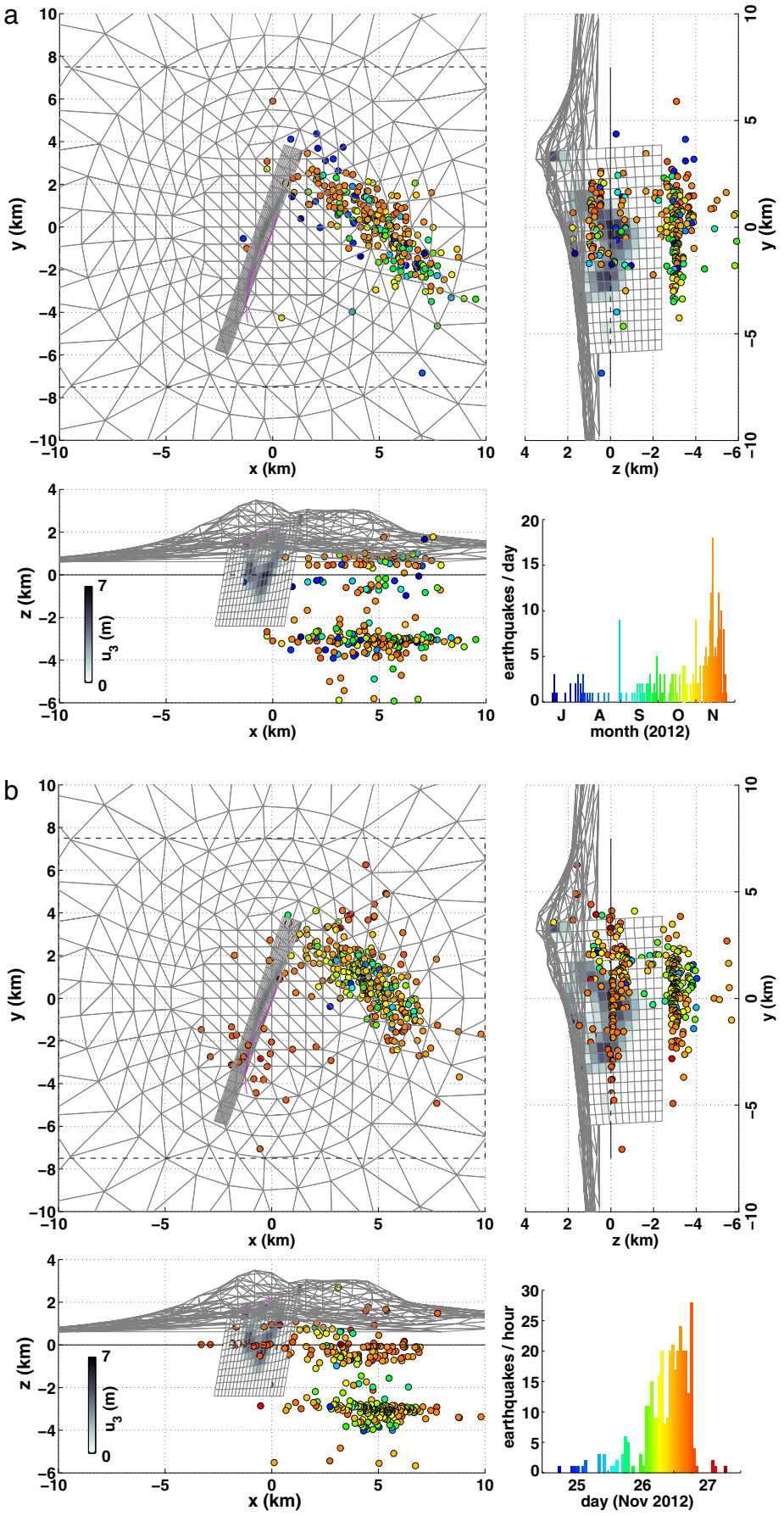

Please cite this article as: Lundgren, P., et al., Dike model for the 2012–2013 Tolbachik eruption constrained by satellite radar interferometry observations, J. Volcanol. Geotherm. Res. (2015), http://dx.doi.org/10.1016/j.jvolgeores.2015.05.011

personal communication]. In contrast, the 1996–1998 inflation of Peulik volcano in the Alaska Peninsula was accompanied during May–October 1998 by a seismic swarm at Becharof Lake, some 30 km from the volcano with no resulting eruption [Lu et al., 2002]. In the case of Tolbachik the lack of an InSAR signature and only distant GPS sites make comparison to previously observed volcano or volcano-tectonic scenarios highly speculative.

Despite the uncertainties regarding interpretation of the seismicity swarm in the months prior to the 2012 eruption we can explore scenarios in which there would have been magma accumulation (and pressurization) present within the area of the seismic swarm. Simple models based on simple-shaped magma pressure volumes beneath the seismicity (Fig. 10b, c) demonstrate that more complex patterns of clamping/unclamping might promote dike opening in the area constrained by the InSAR observations. These models do not account for external extensional stresses nor account for variations in topographic load. The lack of dike propagation farther down-rift toward the 1975 fissures suggests that the dike reached the surface before it could propagate that far, likely due to its confinement to shallower depths.

If we consider the previous two paragraphs, then perhaps we can place some bounds on possible and more likely magma transport models. One scenario (similar to Peulik) would be that magma migrated from depth beneath the central conduit with the SE Tolbachik seismicity simply triggered by the change in stress from central conduit magma reservoirs; again with a rapid enough inflation–deflation sequence that there is no net deformation apparent in the 1-year interferograms spanning the eruption. A second scenario would be the one in Fig. 10b–c in which lateral magma reservoirs would inflate and cause the seismic swarm and also modulate the rift normal stresses, resulting in magma transport high within the Plosky Tolbachik edifice and propagation laterally in the upper rift system. To distinguish between these two scenarios will require analysis of the GPS displacements, assuming they can resolve the source location adequately — a scenario similar to the ongoing inflation at Nevado del Ruiz volcano, Colombia, where InSAR reveals a deep source 10 km SW of the summit [Lundgren et al., in press] and the local GPS network is all located NE of the source but preliminary analysis is able to locate the source reasonably well [Ordoñez et al., 2015]. The shallow seismicity (<10 km depth) of the 2012 eruption compared to the stronger earthquakes and seismic evidence for transport of magma for the GTE (>25 km depth), as well as petrological differences [Edwards et al., 2013], suggests that other analyses of this eruption should help constrain models for magma storage and transport during the 2012 Tolbachik eruption.

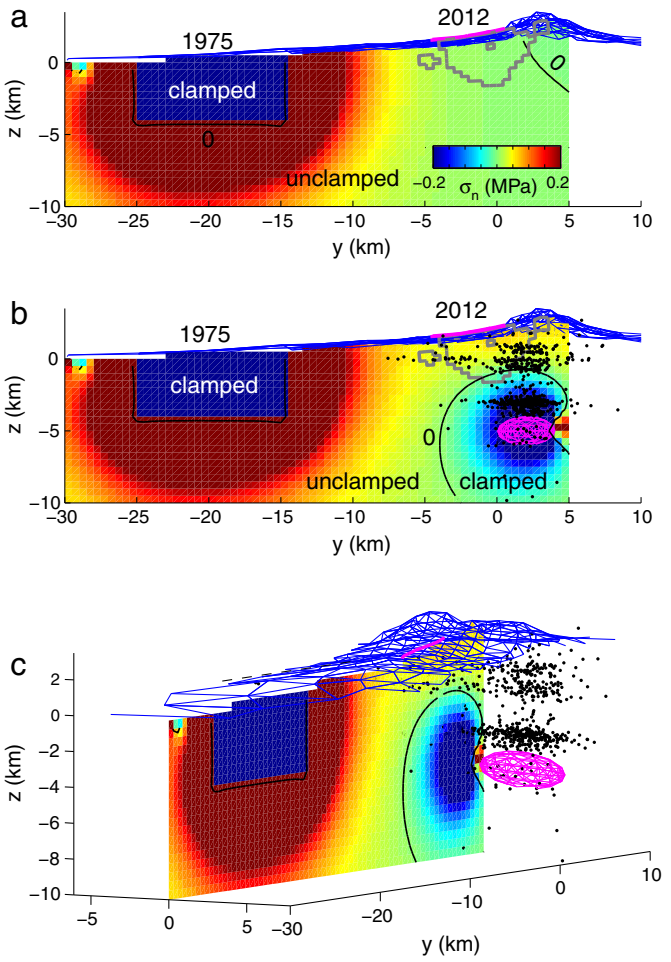

Fig. 10. Stress change normal to the plane of the New Tolbachik rift zone. In this simulation of a dike representing the 1975 GTE intrusion (blue rectangular area of clamping stress change), the dike length extends over the entire span of the 1975–1976 eruptive fissures and is restricted to within 3 km of the surface with 1 m opening. Stress magnitude color scale is saturated at the upper and lower limits. Black curve is the zero contour. Irregular gray line outlines the area of opening in the Gamma = 50 model from this study. Eruptive fissures are shown (magenta line) on top of the surface topography mesh (blue). (a) Model with only the 1975 dike. (b) Model including a 5 km depth spheroidal chamber with 4 km long and 1 km short axes. Excess pressure (ΔP) is 10 MPa. Seismicity is shown as black dots. (c) Perspective view of model with spheroid. Inclusion of one or more magma bodies can modify the normal stress to promote opening in the location of the modeled 2012 dike (and discourage opening at greater depth), whereas the 1975 dike provides only a simple constraint.

6. Conclusions

We compute a distributed dike-opening model for the November 2012 to August 2013 dike intrusion and fissure eruption. Since our data span the entirety of the intrusion and eruption we see the entire process in the InSAR data and cannot determine the space–time progression of dike propagation and opening during the eruption [e.g. Segall et al., 2001, 2013; Rivalta, 2010; Lundgren et al., 2013]. When we take into account topography and force the dike surface to align with the surface fissure eruption centers we find a dip of 80° to the WNW best fits the observations. Maximum dike opening is 6–8 m for reasonable amounts of model Laplacian smoothing. Dike volume is calculated at 44 MCM. The lack of a deeper root to the dike and the band of seismicity that occurs at a similar depth suggests that the dike propagated laterally from the central conduit of Plosky Tolbachik at depths from 1 km below sea level, reaching the eruptive fissures at 1–2 km elevation on the volcano surface.

Supplementary data to this article can be found online at http://dx.doi.org/10.1016/j.jvolgeores.2015.05.011.

Acknowledgments

We thank Dmitry Melnikov for providing digitized lava flow fields for the 2012–2013 Tolbachik eruption, and facilitated by Ben Edwards. We thank the Canadian Space Agency for providing RADARSAT-2 data. Part of this research was carried out using COSMO-SkyMed (CSK®) products delivered under an Italian Space Agency (ASI) license and is made possible through a collaboration between JPL/Caltech/CIDOT and NASA/ASI. Fieldwork was supported by Russia Fund Basic Research grant # 12-05-00125. The research was carried out at the Jet Propulsion Laboratory, California Institute of Technology, under a contract with the National Aeronautics and Space Administration.

Fig. 9. Dike opening model (in gray shading) compared to seismicity. Dike opening is for Gamma 50 model. (a) Seismicity for July 1 through November 24, 2012, color-coded by date during this time interval as shown in histogram plot in the lower right plot in (a). (b) Seismicity during November 25–27, 2012 colored as a function of time over those 3 days as shown in the lower right plot of earthquakes per hour. The peak seismicity (November 27, 07:00 UTC) marks the dike propagation and is followed by a rapid decline in seismicity.

Please cite this article as: Lundgren, P., et al., Dike model for the 2012–2013 Tolbachik eruption constrained by satellite radar interferometry observations, J. Volcanol. Geotherm. Res. (2015), http://dx.doi.org/10.1016/j.jvolgeores.2015.05.011

References

Amelung, F., Yun, S.-H., Walter, T.R., Segall, P., Kim, S.-W., 2007. Stress control of deep rift intrusion at Mauna Loa volcano, Hawaii. Science 316, 1026–1030. http://dx.doi.org/10.1126/science.1140035.

Bagnardi, M., Amelung, F., Poland, M., 2013. A new model for the growth of basaltic shields based on deformation of Fernandina volcano, Galapagos Islands. Earth Planet. Sci. Lett. 377–378, 358–366. http://dx.doi.org/10.1016/j.epsl.2013.07.016.

Churikova, T., Gordeychik, B., Iwamori, H., Nakamura, H., Nishizawa, T., Haraguchi, S., Yasukawa, K., Ishizuka, O., 2014. Petrology and geochemistry of the Tolbachik volcano. Proceedings of the 8th Biennial Workshop on Japan-Kamchatka-Alaska Subduction Processes, http://hkdrcep.sci.hokudai.ac.jp/map/jkasp2014/proglist.html.

Dvigalo, V.N., Fedotov, S.A., Chirkov, A.M., 1991. Plosky Tolbachik, in Active Volcanoes of Kamchatka. vol. 1. Nauka Publishers, Moscow, pp. 210–211.

Edwards, B., Belousov, A., Belousov, M., Volynets, A., Melnikov, D., Chirkov, S., 2013. Another "Great Tolbachik" eruption? Eos. Trans. AGU 94, 189–191.

Fedotov, S.A., Balesta, S.T., Dvigalo, V.N., Razina, A.A., Flerov, G.B., Chirkov, A.M., 1991. New Tolbachik Volcanoes, in Active Volcanoes of Kamchatka. Vol. 1. Nauka Publishers, Moscow, pp. 275–279.

Fukuda, J., Johnson, K.M., 2010. Mixed linear–non-linear inversion of crustal deformation data: Bayesian inference of model, weighting and regularization parameters. Geophys. J. Int. 181, 1441–1458. http://dx.doi.org/10.1111/j.1365-246X.2010.04564.x.

Goldstein, R.M., Werner, C.L., 1998. Radar interferogram filtering for geophysical applications. Geophys. Res. Lett. 25 (21), 4035–4038. http://dx.doi.org/10.1029/1998GL900033.

Goldstein, R.M., Zebker, H.A., Werner, C.L., 1988. Satellite radar interferometry: two-dimensional phase unwrapping. Radio Sci. 23 (4), 713–720. http://dx.doi.org/10.1029/RS023i004p00713.

Gordeev, E.I., Droznin, V.A., Dubrovskaya, I.K., Dvigalo, V.N., Magushkin, M.A., Muravyev, Y., Titkov, N.V., Volynets, A.O., 2014. Proceedings of the 8th Biennial Workshop on Japan–Kamchatka–Alaska Subduction Processes, http://hkdrcep.sci.hokudai.ac.jp/map/jkasp2014/proglist.html.

Gudmundsson, A., 2012. Magma chambers: formation, local stresses, excess pressures, and compartments. J. Volcanol. Geotherm. Res. 237–238, 19–41. http://dx.doi.org/10.1016/j.jvolgeores.2012.05.015.

Jónsson, S., Zebker, H., Segall, P., Amelung, F., 2002. Fault slip distribution of the 1999 Mw 7.1 Hector Mine, California, earthquake, estimated from satellite radar and GPS measurements. Bull. Seismol. Soc. Am. 92, 1377–1389.

Kiryukhin, A.V., Fedotov, S.A., Kiryukhin, P.A., 2015. Geomechanical interpretation of local seismicity before Tolbachik volcano eruption 27.11.2012. Proc. 18th Volcanology Conference, Petropavlovsk-Kamchatsky, pp. 266–269 (in Russian).

Kugaenko, Y.A., Saltykov, V.A., Gorbatikov, A.V., Stepanova, M.Y., 2013. Deep structure of the north vent area, Great Tolbachik fissure eruption of 1975–1976, Kamchatka: evidence from low frequency microseismic sounding. J. Volcanol. Seismol. 7, 313–327. http://dx.doi.org/10.1134/S0742046313050035.

Kugaenko, Y., Saltykov, V., Gorbatikov, A., Stepanova, M., 2014. Estimation of geological structure at Tolbachik Dol (Kamchatka) using low-frequency microseisms. Proceedings of the 8th Biennial Workshop on Japan–Kamchatka–Alaska Subduction Processes, http://hkdrcep.sci.hokudai.ac.jp/map/jkasp2014/proglist.html.

Lin, G., Shearer, P.M., Matoza, R.S., Okubo, P.G., Amelung, F., 2014. Three-dimensional seismic velocity structure of Mauna Loa and Kilauea volcanoes in Hawaii from local seismic tomography. J. Geophys. Res. Solid Earth 119, 4377–4392. http://dx.doi.org/10.1002/2013JB010820.

Lohman, R.B., Simons, M., 2005. Some thoughts on the use of InSAR data to constrain models of surface deformation: noise structure and data downsampling. Geochem. Geophys. Geosyst. 6, Q01007. http://dx.doi.org/10.1029/2004GC000841.

Lu, Z., Wicks Jr., C., Dzurisin, D., Power, J.A., Moran, S.C., Thatcher, W., 2002. Magmatic inflation at a dormant stratovolcano: 1996–1998 activity at Mount Peulik volcano, Alaska, revealed by satellite radar interferometry. J. Geophys. Res. 107, 2134. http://dx.doi.org/10.1029/2001JB000471.

Lundgren, P., Lu, Z., 2006. Inflation model of Uzon caldera, Kamchatka, constrained by satellite radar interferometry observations. Geophys. Res. Lett. 33, L063012. http://dx.doi.org/10.1029/2005GL025181.

Lundgren, P., Poland, M., Miklius, A., Orr, T., Yun, S.-H., Fielding, E., Liu, Z., Tanaka, A., Szeliga, W., Hensley, S., Owen, S., 2013. Evolution of dike opening during the March 2011 Kamoamoa fissure eruption, Kilauea Volcano, Hawai'i. J. Geophys. Res. Solid Earth 118. http://dx.doi.org/10.1002/jgrb.50108.

Lundgren, P., Milillo, P., Mothes, P., Medina, L.N., Laverde, C., Wessels, R., Amelung, F., Samsonov, S., Tanaka, A., Owen, S., Biggs, J., Ebmeier, S.K., Parker, A., Battaglia, M., Prejean, S., Lyons, J., 2015. The Chiles — Cerro Negro Volcanoes Unrest: Application of InSAR, In-situ Geodesy, and Other Observations to an Evolving Crisis, Fringe 2015 Advances in the Science and Applications of SAR Interferometry and Sentinel-1 InSAR Workshop (http://seom.esa.int/fringe2015/page_session25.php).

Lundgren, P., Samsonov, S.V., Velez, C.M.L., Ordoñez, M., 2015. Deep source model for Nevado del Ruiz Volcano, Colombia, constrained by InSAR observations. Geophys. Res. Lett. in press.

Malinverno, A., 2002. Parsimonious Bayesian Markov chain Monte Carlo inversion in a nonlinear geophysical problem. Geophys. J. Int. 151, 675–688.

Masterlark, T., Haney, M., Dickinson, H., Fournier, T., Searcy, C., 2010. Rheologic and structural controls on the deformation of Okmok volcano, Alaska: FEMs, InSAR, and ambient noise tomography. J. Geophys. Res. 115, B02409. http://dx.doi.org/10.1029/2009JB006324.

Matoza, R.S., Shearer, P.M., Lin, G., Wolfe, C.J., Okubo, P.G., 2013. Systematic relocation of seismicity on Hawaii Island from 1992 to 2009 using waveform cross correlation and cluster analysis. J. Geophys. Res. Solid Earth 118, 2275–2288. http://dx.doi.org/10.1002/jgrb.50189.

Mosegaard, K., Tarantola, A., 2002. Probabilistic approach to inverse problems. International Handbook of Earthquake and Engineering Seismology, Part A. Academic, San Diego, Calif, pp. 237–265.

Okada, Y., 1985. Surface deformation due to shear and tensile faults in a halfspace. Bull. Seismol. Soc. Am. 75, 1135–1154.

Ordoñez, M., López, C., Alpala, J., Narváez, L., Arcos, D., Battaglia, M., 2015. Keeping watch over Colombia's slumbering volcanoes. Eos 96. http://dx.doi.org/10.1029/2015EO025079.

Owen, S., Segall, P., Lisowski, M., Miklius, A., Murray, M., Bevis, M., Foster, J., 2000. January 30, 1997 eruptive event on Kilauea Volcano, Hawaii, as monitored by continuous GPS. Geophys. Res. Lett. 27 (17), 2757–2760. http://dx.doi.org/10.1029/1999GL008454.

Rivalta, E., 2010. Evidence that coupling to magma chambers controls the volume history and velocity of laterally propagating intrusions. J. Geophys. Res. 115, B07203. http://dx.doi.org/10.1029/2009JB006922.

Rivalta, E., Segall, P., 2008. Magma compressibility and the missing source for some dike intrusions. Geophys. Res. Lett. 35, L04306. http://dx.doi.org/10.1029/2007GL032521.

Rosen, P.A., Hensley, S., Joughin, I.R., Li, F.K., Madsen, S.N., Rodriguez, E., Goldstein, R.M., 2000. Synthetic aperture radar interferometry. Proc. IEEE 88, 333–382.

Salzer, J.T., Nikkhoo, M., Walter, T.R., Sudhaus, H., Reyes-Dávila, G., Bretón, M., Arámbula, R., 2014. Satellite radar data reveal short-term pre-explosive displacements and a complex conduit system at Volcán de Colima. Mexico Front. Earth Sci. 2, 12. http://dx.doi.org/10.3389/feart.2014.00012.

Segall, P., Cervelli, P., Owen, S., Lisowski, M., Miklius, A., 2001. Constraints on dike propagation from continuous GPS measurements. J. Geophys. Res. 106 (B9), 19,301–19,317.

Segall, P., Llenos, A.L., Yun, S.-H., Bradley, A.M., Syracuse, E.M., 2013. Time-dependent dike propagation from joint inversion of seismicity and deformation data. J. Geophys. Res. Solid Earth 118, 5785–5804. http://dx.doi.org/10.1002/2013JB010251.

Shearer, P., Hauksson, E., Lin, G.Q., 2005. Southern California hypocenter relocation with waveform cross-correlation, Part 2: results using source-specific station terms and cluster analysis. Bull. Seismol. Soc. Am. 95, 904–915.

Sigmundsson, F., Hooper, A., Hreinsdóttir, S., Vogfjörd, K.S., Ófeigsson, B.G., Heimisson, E.R., Dumont, S., Parks, M., Spaans, K., Gudmundsson, G.B., Drouin, V., Árnadóttir, T., Jónsdóttir, K., Gudmundsson, M.T., Högnadóttir, T., Fridriksdóttir, H.M., Hensch, M., Einarsson, P., Magnússon, E., Samsonov, S., Brandsdóttir, B., White, R.S., Ágústsdóttir, T., Greenfield, T., Green, R.G., Hjartardóttir, Á.R., Pedersen, R., Bennett, R.A., Geirsson, H., La Femina, P.C., Björnsson, H., Pálsson, F., Sturkell, E., Bean, C.J., Möllhoff, M., Braiden, A.K., Eibl, E.P.S., 2015. Segmented lateral dyke growth in a rifting event at Bárdarbunga volcanic system. Iceland. Nature 517, 191–195. http://dx.doi.org/10.1038/nature14111.

Thomas, A.L., 1993. Poly3D: a three-dimensional, polygonal element, displacement discontinuity boundary element computer program with applications to fractures, faults, and cavities in the Earth's crust M.S. thesis, Stanford Univ, Stanford, Calif (221 pp.).

Volynets, A.O., Melnikov, D.V., Yakushev, A.I., 2013. First data on composition of the volcanic rocks of the IVS 50th anniversary Fissure Tolbachik eruption (Kamchatka). Dokl. Earth Sci. 452 (1), 953–957. http://dx.doi.org/10.1134/S1028334X13090201.

Walter, T.R., Amelung, F., 2006. Volcano-earthquake interaction at Mauna Loa volcano, Hawaii. J. Geophys. Res. 111, B05204. http://dx.doi.org/10.1029/2005JB003861.

Wegmuller, U., Werner, C., 1997. Gamma SAR Processor and Interferometry Software, The 3rd ERS Symposium on Space at the Service of Our Environment. Florence, Italy.

Wessel, P., Smith, W.H.F., 1995. New version of the generic mapping tools released. Eos. Trans. AGU 76, 329.

Williams, C.A., Wadge, G., 2000. An accurate and efficient method for including the effects of topography in three-dimensional elastic models of ground deformation with application to radar interferometry. J. Geophys. Res. 105, 8103–8120.

Wright, T.J., Ebinger, C., Biggs, J., Ayele, A., Yirgu, G., Keir, D., Stork, A., 2006. Magma-maintained rift segmentation at continental rupture in the 2005 Afar dyking episode. Nature 442, 291–294. http://dx.doi.org/10.1038/nature04978.

Yun, S., Segall, P., Zebker, H., 2006. Constraints on magma chamber geometry at Sierra Negra Volcano, Galápagos Islands, based on InSAR observations. J. Volcanol. Geotherm. Res. 150 (1), 232–243.

Zoback, M.D., 2010. Reservoir Geomechanics. Cambridge University Press (448 p).

Please cite this article as: Lundgren, P., et al., Dike model for the 2012–2013 Tolbachik eruption constrained by satellite radar interferometry observations, J. Volcanol. Geotherm. Res. (2015), http://dx.doi.org/10.1016/j.jvolgeores.2015.05.011